

Investigation of realistic PET simulations incorporating tumor patient's specificity using anthropomorphic models: Creation of an oncology database

Panagiotis Papadimitroulas

Department of Medical Physics, School of Medicine, University of Patras, Rion, GR 265 04, Greece

George Loudos

Department of Biomedical Engineering, Technological Educational Institute of Athens, Ag. Spyridonos Street, Egaleo GR 122 10, Athens, Greece

Amandine Le Maitre, Mathieu Hatt, and Florent Tixier

Medical Information Processing Laboratory (LaTIM), National Institute of Health and Medical Research (INSERM), 29609 Brest, France

Nikos Efthimiou and George C. Nikiforidis

Department of Medical Physics, School of Medicine, University of Patras, Rion, GR 265 04, Greece

Dimitris Visvikis

Medical Information Processing Laboratory (LaTIM), National Institute of Health and Medical Research (INSERM), 29609 Brest, France

George C. Kagadis^{a)}

Department of Medical Physics, School of Medicine, University of Patras, Rion, GR 265 04, Greece

(Received 12 March 2013; revised 3 October 2013; accepted for publication 4 October 2013; published 28 October 2013)

Purpose: The GATE Monte Carlo simulation toolkit is used for the implementation of realistic PET simulations incorporating tumor heterogeneous activity distributions. The reconstructed patient images include noise from the acquisition process, imaging system's performance restrictions and have limited spatial resolution. For those reasons, the measured intensity cannot be simply introduced in GATE simulations, to reproduce clinical data. Investigation of the heterogeneity distribution within tumors applying partial volume correction (PVC) algorithms was assessed. The purpose of the present study was to create a simulated oncology database based on clinical data with realistic intratumor uptake heterogeneity properties.

Methods: PET/CT data of seven oncology patients were used in order to create a realistic tumor database investigating the heterogeneity activity distribution of the simulated tumors. The anthropomorphic models (NURBS based cardiac torso and Zubal phantoms) were adapted to the CT data of each patient, and the activity distribution was extracted from the respective PET data. The patient-specific models were simulated with the Monte Carlo Geant4 application for tomography emission (GATE) in three different levels for each case: (a) using homogeneous activity within the tumor, (b) using heterogeneous activity distribution in every voxel within the tumor as it was extracted from the PET image, and (c) using heterogeneous activity distribution corresponding to the clinical image following PVC. The three different types of simulated data in each case were reconstructed with two iterations and filtered with a 3D Gaussian postfilter, in order to simulate the intratumor heterogeneous uptake. Heterogeneity in all generated images was quantified using textural feature derived parameters in 3D according to the ground truth of the simulation, and compared to clinical measurements. Finally, profiles were plotted in central slices of the tumors, across lines with heterogeneous activity distribution for visual assessment.

Results: The accuracy of the simulated database was assessed against the original clinical images. The PVC simulated images matched the clinical ones best. Local, regional, and global features extracted from the PVC simulated images were closest to the clinical measurements, with the exception of the size zone variability and the mean intensity values, where heterogeneous tumors showed better reproducibility. The profiles on PVC simulated tumors after postfiltering seemed to represent the more realistic heterogeneous regions with respect to the clinical reference.

Conclusions: In this study, the authors investigated the input activity map heterogeneity in the GATE simulations of tumors with heterogeneous activity distribution. The most realistic heterogeneous tumors were obtained by inserting PVC activity distributions from the clinical image into the activity map of the simulation. Partial volume effect (PVE) can play a crucial role in the quantification of heterogeneity within tumors and have an important impact on applications such as patient follow-up during treatment and assessment of tumor response to therapy. The development

of such a database incorporating patient anatomical and functional variability can be used to evaluate new image processing or analysis algorithms, while providing control of the ground truth, which is not available when dealing with clinical datasets. The database includes all images used and generated in this study, as well as the sinograms and the attenuation phantoms for further investigation. It is freely available to the interested reader of the journal at <http://www.med.upatras.gr/oncibase/>. © 2013 American Association of Physicists in Medicine. [<http://dx.doi.org/10.1118/1.4826162>]

Key words: tumor heterogeneity, realistic simulations, GATE, PET database, anthropomorphic phantoms

1. INTRODUCTION

Positron emission tomography (PET) is considered the state of the art for oncology diagnosis and treatment planning and ^{18}F -FDG is the most widely used radiotracer in such applications.¹ Optimization of quantification of PET images in clinical practice is also a field of intense interest and research to fully exploit functional information of this technique.

Over the past years the introduction of computer science in the field of medical physics has been rapidly evolving. Monte Carlo (MC) simulations are increasingly being used in nuclear medicine as a tool that could soon be translated in the clinical practice. The Geant4 applications for tomography emission (GATE) MC toolkit provides high accuracy in physics modeling and is optimized for nuclear imaging applications, with large flexibility in using voxelized phantoms and complex geometries, allowing movement incorporation.^{2,3} Compared to other MC packages, GATE offers additional precision considering physics modeling, which is handled by the Geant4 code^{4,5} and it has been extensively validated both on simple and more realistic geometries, which are highly demanding in computational resources. MC simulations of PET acquisitions are still the most reliable approaches to validate and assess the performance of image processing/analysis or reconstruction algorithms, such as (i) partial volume correction (PVC), (ii) de-noising, (iii) segmentation, (iv) reconstruction, and (v) automated detection. MC simulations provide the ground truth of the input data, since they allow total control of interactions taking place. Thus, they can either provide artifact free data, to validate correction algorithms or allow the execution of biased experiments to understand and quantify the effect of a process on acquired data.

Simulated emission tomography images have been widely used for the evaluation and the validation of processing methods and acquisition protocols used in clinical practice.⁶⁻⁹ Previous studies have presented simulated PET databases for such purposes. Reihl *et al.*¹⁰ proposed a cerebral PET database based on the PET-SORTEO MC code. With the same MC tool a database of FDG PET images for lymphoma was proposed by Tomei *et al.*¹¹ A large database containing several cases of emission tomography simulated brain and whole body data was proposed by Castiglioni *et al.*¹² in 2005. Recently, an open access database containing simulated PET-MR datasets based on real MR acquisitions was made available by King's College London.¹³ Although GATE is highly accepted in the nuclear imaging community, at the moment

there is no GATE based PET database available, which could be used as a reference dataset regarding the simulation of realistic tumors with complex shapes and heterogeneous activity distributions. Two recent studies investigated the simulation of realistic PET images. The first introduced the use of variability in the phantoms in order to generate various anatomies, and the use of complex shapes and different levels of activity in the tumors in order to generate realistic tumors.¹⁴ However, this study only investigated the use of a limited number of activity levels in a tumor to generate heterogeneity. A more recent study by Stute *et al.*¹⁵ demonstrated the feasibility of highly realistic simulations of PET images including tumors and accounting for the heterogeneous uptake throughout the body. Another recent study investigated the impact of the input data on the simulated images and it suggested using input data with very high spatial resolution in order to best reproduce the clinical images with the MC techniques.¹⁶ In the study of Stute *et al.*, ^{18}F -FDG PET and ^{131}I SPECT scans were acquired testing the propagation of the noise and spatial resolution in the input activity distribution for realistic simulated data. Real patients' scans were used in the simulations while the results showed that the noise properties of the reconstructed simulated images were almost independent of the noise input activity distribution. However, using high-noise and high-resolution patient data as input yielded reconstructed images that could not be distinguished from clinical images. Subtle differences between the reconstructed volumes suggest that a very high level of noise might impact some small structures with heterogeneous activity distribution.

The main goal of the present study was to create a PET database with realistic tumor simulations, incorporating both patient variability within anthropomorphic computational models and highly realistic and validated intratumor tracer uptake heterogeneity incorporating patient's anatomical and functional characteristics. The impact of several parameters playing a role in clinical routine PET imaging was also investigated.

2. MATERIALS AND METHODS

This study incorporates the patient's variability using anthropomorphic computational models. The Philips Allegro and the Siemens Biograph-6 PET scanners, already modeled in the GATE MC platform, were used in the presented database.^{17,18} The NCAT and Zubal phantoms were used for simulating different patients. PET/CT clinical data were

used for the extraction of the activity distribution and the attenuation map. The simulated data were reconstructed using the STIR software.¹⁹ A database of seven different clinical studies was created and quantitative analysis was performed between the simulated and clinical images to evaluate simulation realism. The simulation procedure was divided in two main parts. The first one is the modeling of the scanner and the second one incorporates the description of the voxelized phantoms (including attenuation and activity maps). The whole procedure is explained in Secs. 2.A–2.D.

2.A. GATE Monte Carlo toolkit

This study was based on the GATE v6.0 release using the Geant4.9.4 code.^{2,4} All the appropriate physical processes needed for realistic simulations were modeled using the “standard model.”

2.B. Clinical data

The simulated database is based on clinical PET/CT real data acquired on a Philips PET/CT Allegro/GEMINI system (Philips Medical Systems, Cleveland, OH, USA). Patients fasted for at least 6 h before injection. The dose of administered ¹⁸F-DG was 5 MBq/kg with a postinjection average of 60 min. CT data were acquired first (120 kV and 100 mAs, no contrast-enhancement). 3D PET data were acquired with 2 min per bed position, and images were reconstructed using CT based attenuation correction and a 3D row-action maximum likelihood algorithm (RAMLA) using a previously optimized protocol (two iterations, $4 \times 4 \times 4$ mm³ voxels grid sampling, 5 mm 3D Gaussian postfiltering, relaxation parameter of 0.05).²⁰ The seven oncological cases included different types of tumors. Specifically, three lung tumors (patients 1–3), one lymphoma in the ORL region (patient 4), and three head-brain tumors (patients 5–7) were modeled.

In the present study, we used the same scanner model for executing the simulations in order to have more comparable results to the clinical data. However, in the database a second dataset of the seven oncology patients is also included using the Biograph-6 PET system.

2.C. Data preparation

2.C.1. Attenuation phantom

The anatomy of the patients in our study was modeled using the nonuniform rational basis splines (NURBS)-based cardiac-torso (NCAT) and the CT-based head Zubal phantoms.^{21–24} The NCAT phantom provides very good flexibility for the creation of realistic organ models due to the NURBS surfaces. The NCAT phantom was adapted to the first three patient’s anatomy (patients 1, 2, and 3) with information from the corresponding CT data using an interactive software application.^{25,26} 2D slices of the NCAT phantom were overlaid with corresponding slices of the CT images. The organ shapes were modified by changing the position of the control points associated to the NURBS surfaces of each organ. Rotations, translations, and scaling were applied to one or several organs, in order to achieve a global adaptation of the phantom to the anatomy of a given patient. For the last four cases, the Zubal head phantom was used, in order to simulate the tumors within them. In those four cases, the Zubal phantom was not modified; instead only the tumor location was different across the different simulations.

For the attenuation map, the attenuation coefficients at 511 keV photon energy of NIST (Ref. 27) were used for the different organs participating in each simulation. The various organs in each phantom were simulated with the materials provided by the GATE Materials Database (Materials.db) (Ref. 3), namely, air, lung, body, ribbone, spinebone, intestine, breast, spleen, blood, heart, liver, kidney, water, softtissue, adipose, brain, skull, and muscle. The tumors in the simulations were considered as soft tissue media.

The phantoms imported in GATE had a voxel scaling of $4 \times 4 \times 4$ mm³, equal to the crystal size of the modeled scanner. Details for all the phantoms and the simulation acquisitions are given in Table I of the Appendix.

2.C.2. Activity map

The activity distributions were inserted in the GATE software by defining the activity value of each individual voxel (in Bq). The exact SUV values of each voxel were calculated based on the clinical PET data.¹⁴ The ¹⁸F-FDG distribution was extracted from the individual patient clinical data. Regions of interest (ROIs) were defined in the various organs

TABLE I. Information for the clinical data and the phantoms imported in GATE.

	Clinical data matrix	Computational model	Phantom voxel size	Tumor voxels	Tumor activity (MBq)	Total inserted activity (MBq)
Patient 1	144 × 144 × 192	NCAT	4 × 4 × 4	631	0.68	34.50
Patient 2	144 × 144 × 234	NCAT	4 × 4 × 4	1640	0.72	57.41
Patient 3	144 × 144 × 212	NCAT	4 × 4 × 4	3185	11.15	82.87
Patient 4	144 × 144 × 211	Zubal	4 × 4 × 4	1025	0.67	25.61
Patient 5	128 × 128 × 93	Zubal	4 × 4 × 4	3068	4.21	29.03
Patient 6	128 × 128 × 47	Zubal	4 × 4 × 4	842	0.88	25.85
Patient 7	128 × 128 × 47	Zubal	4 × 4 × 4	893	1.03	25.97

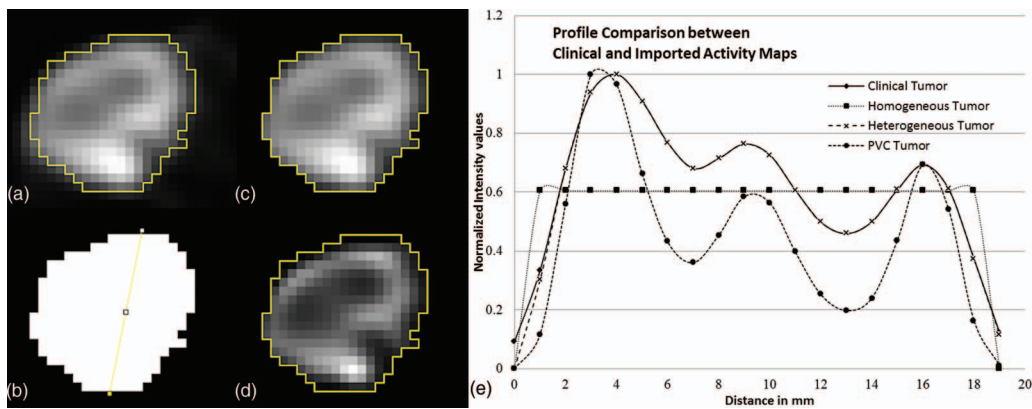


FIG. 1. Representation of the activity distribution within the central slice of the patient 5 tumor: (a) clinical, (b) homogeneous, (c) heterogeneous, and (d) PVC activity distribution. Cases (b)–(d) are the different inputs in the simulation for one patient. The normalized profiles in these four cases are presented in (e) where the values are normalized to the maximum value of this slice.

(liver, lung, kidneys, etc.) to calculate the activity concentrations per organ. Then, the activity concentrations were compared to the theoretical standard uptake values (SUVs) that already exist in the literature.²⁸

2.C.3. Tumor modeling

In order to investigate the tumor activity distribution, the clinical tumors were inserted in the computational phantoms. Our purpose was to investigate the realism of the simulated heterogeneity activity distribution in the reconstructed images with respect to the actual distribution inserted in the simulated phantom. The anthropomorphic phantoms were prepared as discussed in Secs. 2.C.1 and 2.C.2 without modeling any abnormality of the patient. The exact tumor shape on each individual patient was then extracted from the clinical image and imported in the corresponding phantom.

Initially the tumors were automatically delineated using the fuzzy locally adaptive Bayesian algorithm from the clinical PET images.²⁹ Resulting segmentation masks were checked visually to ensure the entire functional PET uptake distribution was well included. A mask of the tumor was created for each patient defining the shape of the tumor based on the delineation result, representing the ground truth for our simulations. The assessment and comparison of the heterogeneity distribution visual appearance and quantification within the tumor was carried out by defining three different activity maps for the ground truth. The most simple consisted in extracting the mean activity value within the delineated tumor on the clinical PET images, and assigning it to a homogeneous activity distribution. These simulations will be denoted as “homogeneous” from here onwards. A second series of simulations were performed by using heterogeneous activity maps inside the tumors. The activity in each voxel of the simulated ground truth was defined with exactly the same value as in the corresponding clinical image (voxel-by-voxel heterogeneity distribution). These simulations will be denoted as “heterogeneous” from here onwards. Finally, activity maps corresponding to the clinical distribution after PVC within the

tumors were also used. These will be denoted as “PVC” simulations from here onwards.

2.C.3.a. Partial volume effects correction. Partial volume effects (PVE) are a consequence of the limited spatial resolution of PET scanners [about 5–6 mm full width at half maximum (FWHM)]. This effect is major especially in tumor imaging, which concerns structures of one to several cm in diameter. In addition, tumor subvolumes and heterogeneities may be smaller.³⁰ Several techniques have been reported in the literature for PVC compensation in emission tomography.^{6,31–34} In our study, we used an iterative deconvolution improved by a wavelet-based denoising previously validated for PET imaging.³⁵

Figure 1 illustrates the three different simulated inputs for one of the simulated tumors along with the clinical original image. A line profile comparison between them is also depicted. These profiles provide an indication of the differences in the activity maps that were imported into GATE.

2.C.4. Simulation procedure

2.C.4.a. Scanner description. The simulations were carried out using a model of the Philips Allegro PET scanner which had already been fully validated for the GATE platform.¹⁷ The whole scanner consists of 28 flat blocks, of 22 by 29 Gadolinium Oxyorthosilicate (GSO) crystals (638 crystals per block). The surface area and the thickness of the individual crystals are $4 \times 6 \times 20 \text{ mm}^3$. The scanner has an axial field of view (FOV) of 18.0 cm and a radial FOV (patient’s port) of 56.0 cm. Moreover, an energy window between 350 and 650 keV was applied via the Thresholder and the Upholder modules, while the energy blurring (blurring resolution) was set to 15% of 511 keV. Finally, the coincidence time window of the scanner was set to 7.5 ns via the coincidence sorter.

2.C.4.b. Acquisition process. One bed position was simulated for each case studied, including the tumor in the specified FOV. Two minutes acquisition time was set according to the clinical protocol procedure.

TABLE II. Number of coincidences (trues, scattered, and random) for the seven simulated patients.

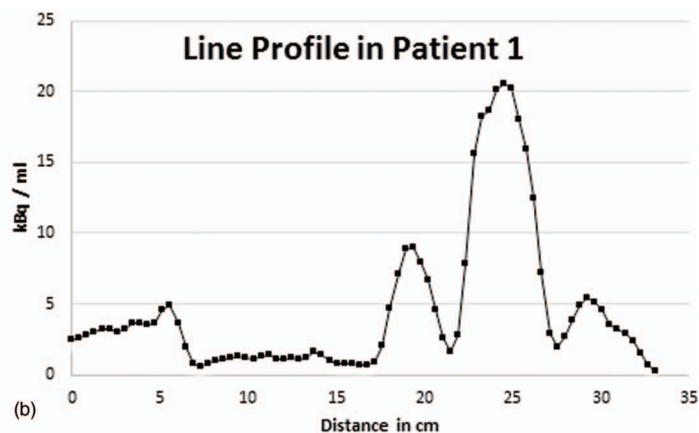
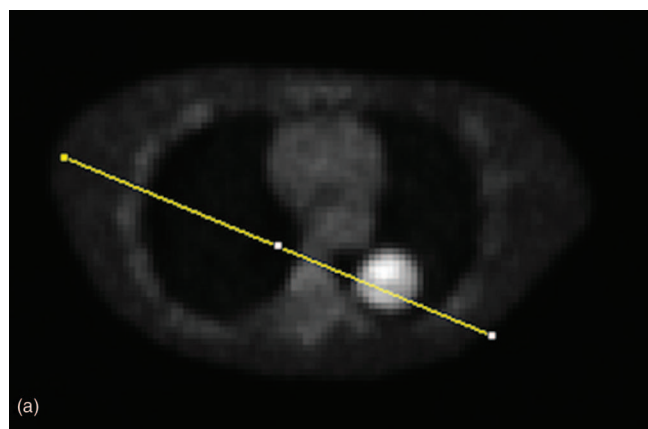
	Number of trues	Scattered	Randoms
Patient 1	16 623 574	30%	38%
Patient 2	28 792 096	25%	49%
Patient 3	36 523 359	35%	35%
Patient 4	8 129 216	33%	37%
Patient 5	8 799 169	29%	24%
Patient 6	6 018 485	32%	26%
Patient 7	9 710 226	42%	25%

GATE v6.0 was used. GATE offers additional precision considering the physics modeling, although it is more computationally demanding than other simulation platforms such as SimSET (Ref. 7) and SORTEO (Ref. 36) that have been previously used for realistic simulations.¹⁴ The simulations were executed in the GateLab grid, which uses parallel computers on the European Grid Infrastructure (EGI).^{37,38} Five hundred processors were used per simulation, with every simulation lasting for about 15 h. Running the simulations in parallel CPUs gave us the opportunity of implementing the acquisitions without any limitations in physical cuts or in using variance reduction techniques (VRTs), achieving good statistics required as in the case of clinical protocols.

The simulated images were reconstructed using only the true coincidences, to obtain data with ideal random and scatter correction. Random and scattered coincidences were excluded from the reconstruction procedure, in order to isolate the information of the “ideal” heterogeneous distribution and to investigate the tumor heterogeneity based on the ground truth of the phantom and the applied MC method. In Table II

the number of the true, scattered and random coincidences are presented for all the patients (homogeneous case).

2.C.4.c. Simulated data processing—OncoBase. The STIR (software for tomography image reconstruction) open-source software (version 2.2) was used for the reconstruction of the simulated data with the OSMAPOSL iterative algorithm (with SPAN 3), which is the implementation of the ordered subset expectation maximization (OSEM) version of Green’s MAP one step late algorithm.³⁹ The Allegro system by Philips was also simulated in the STIR program for the reconstruction of the simulated sinograms. Data were reconstructed using two iterations. All reconstructed images resulting from the STIR software were $128 \times 128 \times 57$ pixels, with pixel spacing $4 \times 4 \times 3.15 \text{ mm}^3$. The 29 crystals of the scanner ($4 \times 4 \text{ mm}^2$ crystal size) resulted in 57 slices in the reconstructed images with the pixel half scaling. Linear interpolation was therefore applied to the data, in order to be directly comparable to the clinical ones (the voxel scaling in the clinical data was $4 \times 4 \times 4 \text{ mm}^3$). All reconstructed images were postsmoothed using a 3D Gaussian filter with a 5 mm FWHM in order to be more comparable with the clinical data that was similarly filtered. Moreover, the database includes data from the Siemens Biograph-6 PET scanner. This system was also modeled in the STIR software resulting in images with $149 \times 149 \times 78$ pixels ($4 \times 4 \times 2 \text{ mm}^3$). In order to extend the database, the dataset of the Biograph-6 includes reconstructed images of the seven patients with one and two iterations, with and without post filtering, for further investigation in processing algorithms. In Figs. 2 and 3 of the Appendix, two patients of the database are presented. In Fig. 2 a central image plane (including the tumor) of patient 1 is shown. For the validation of the process, the simulated plane [Fig. 2(a)] and its line profile is presented in kBq/ml.



Organs	Mean Activity \pm SD (kBq / ml)		
	Current study	Tomei <i>et al.</i> ¹¹	Le Maitre <i>et al.</i> ¹⁴
Tumor	23.59 ± 2.71	-	-
Lungs	1.31 ± 0.24	1.34 ± 0.48	2.08 ± 0.49
Muscle	2.66 ± 0.33	2.58 ± 0.68	-
Liver	9.93 ± 1.31	5.95 ± 1.31	11.97 ± 1.60
Contrast	Simulated	Clinical	
(c) Tumor/Lungs*	18.01	17.55	

FIG. 2. (a) Simulated central axial plane of patient 1 including the tumor, (b) line profile of patient 1 in kBq/ml, and (c) mean activities (kBq/ml) in several organs compared to published data (*in the current study the tumor over lung contrast has been calculated in both clinical and simulated data).

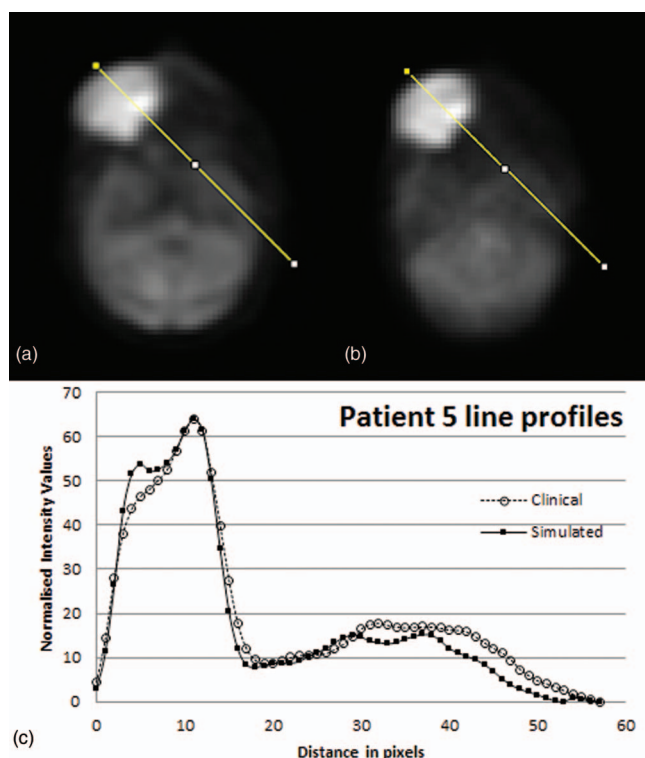


FIG. 3. (a) Clinical case: sum of axial planes of patient 5, (b) simulated case: sum of axial planes of patient 5 (PVC), and (c) line profiles across the head including the tumor area.

The mean activities of the simulated organs of patient 1 were calculated with their associated standard deviation (SD) and are presented in Fig. 2(c). In order to validate the realism of our simulations the results of the mean activity in several organs were compared in Fig. 2(c) to previously published data.^{11,14} Quantitative results of the organs showed the very good agreement of our simulations with other realistic simulations. Furthermore, the simulated tumor-to-lung contrast was compared to the clinical one, showing a difference of 2.55%. In Fig. 3, patient 5 is presented with additional line profiles across the tumor and brain for comparison purposes between the clinical and the simulated images. Through this comparison, the tumor-to-brain contrast was investigated across the two images. Comparing point-by-point the two line profiles, differences ranged between 0% to 36%, with an average difference of $15.01\% \pm 10.91\%$.

The entire database consists of seven different oncological cases and two different scanners. It includes the original clinical PET data for every patient, the mask of the tumor in every case (which represents the ground truth of the tumor), the sinograms in a format suitable for the STIR software, and finally, the simulated data of every case. The simulated data include the three activity maps that were previously described (homogeneous, heterogeneous, and PVC), for every patient. The exact position of every tumor within the phantoms is also provided for every patient.

In order to investigate the simulated intratumor heterogeneity, quantitative analysis is performed in the simulated data of the Allegro system, with two iterations in the recon-

struction algorithm and 5 mm 3D Gaussian postfiltering. All the other cases including the raw data, the sinograms, and the reconstructions are available in the developed database, which is freely available to the interested reader of the journal at <http://www.med.upatras.gr/oncobase/>.

2.D. Image analysis/comparison

Each tumor in the reconstructed images from the raw simulated data was compared to the clinical tumor using several figures of merit in order to identify the most realistic result. In order to compare the simulated intratumor heterogeneity, all the data were normalized according to formula (1) in the same grayscale values (0–64).

$$(I_n - \min(I)) \times \left(\frac{\max T_N - \min T_N}{\max(I) - \min(I)} + \min(I) \right), \quad (1)$$

where I_n is every value of the matrix of the image (I), $\min T_N$ is the minimum value of the new grayscale range (0), $\max T_N$ is the maximum value of the new grayscale range (64), $\min(I)$ is the minimum value of the image, and $\max(I)$ is the maximum value of the image.

First, profiles were drawn across the tumors for visual and qualitative assessment. Second, quantitative measures were automatically extracted and compared across all simulated images with respect to the clinical one. We considered a mixture of global standard tumor quantification parameters (mean activity, standard deviation, and kurtosis) as well as some textural features parameters recently proposed to quantify local (entropy, homogeneity, and dissimilarity), and regional (intensity variability and size zone variability) uptake heterogeneity. The reconstructed (two iterations), postfiltered simulated data were compared to the clinical ones.

2.D.1. Heterogeneity textural features

Textural analysis was performed in our simulated data for the heterogeneity characterization in ^{18}F -FDG images. In two recent studies,^{40,41} the robustness (with respect to acquisition and reconstruction protocols) and physiological reproducibility (assessed on double baseline PET scans) of several textural features for tracer uptake heterogeneity quantification was assessed. Among all the parameters that can be obtained from textural features analysis, the most robust and reproducible were entropy, homogeneity, and dissimilarity (for local characterization) as well as the size and the intensity variability (for regional characterization). These features were therefore chosen to quantify heterogeneity in the present study.

2.D.1.a. Local features. All characteristics were extracted by normalizing the images in 64 levels grayscale. Normalization is required in the same grayscale range in order to have comparable feature values. Entropy, homogeneity, and dissimilarity were extracted for all the images (clinical and simulated) as they are the most stable in reproduction.¹⁷ In order to extract these features, co-occurrence matrices were calculated according to the study of Tixier *et al.*⁴². Local entropy

and homogeneity are defined according to Eqs. (2) and (3), respectively:

$$\text{Entropy} = - \sum_{i,j} M1(i, j) \log(M(i, j)), \quad (2)$$

$$\text{Homogeneity} = \sum_{i,j} \frac{M1(i, j)}{1 + |i - j|}, \quad (3)$$

where $M1$ is a co-occurrence matrix, i, j refer to the specific cell coordinates on the matrix and $M1(i, j)$ is an element of the matrix.

2.D.1.b. Regional features. According to Tixier *et al.*,⁴⁰ the most stable regional features are intensity and size zone variability. The area under the curve (AUC) index is also tested in the present study, which describes the area under a cumulative SUV-volume histograms curve (CSH). It is a quantitative index of tumor uptake heterogeneity, with lower AUC values corresponding to higher degrees of heterogeneity.⁴³

2.D.1.c. Global features. The reproducibility of the global features was previously analyzed,⁴⁰ in accordance to which the SUV mean value and the kurtosis are the most stable parameters. In the present study, the kurtosis and the mean intensity value were extracted for each patient. All simulated data were also compared voxel by voxel to the clinical tumor and the calculated mean difference is presented. All the images were also normalized in the same grayscale range (0–64) in the area of the tumor, in order to extract comparable global features.

3. RESULTS

3.A. Heterogeneity tumor distribution

In this section, the effect of the activity distribution within the tumor is investigated for the variable simulation parameters. Line profiles were selected in representative central slices of the tumor, in which different areas of heterogeneity appear. In Fig. 4, all simulated cases with and without

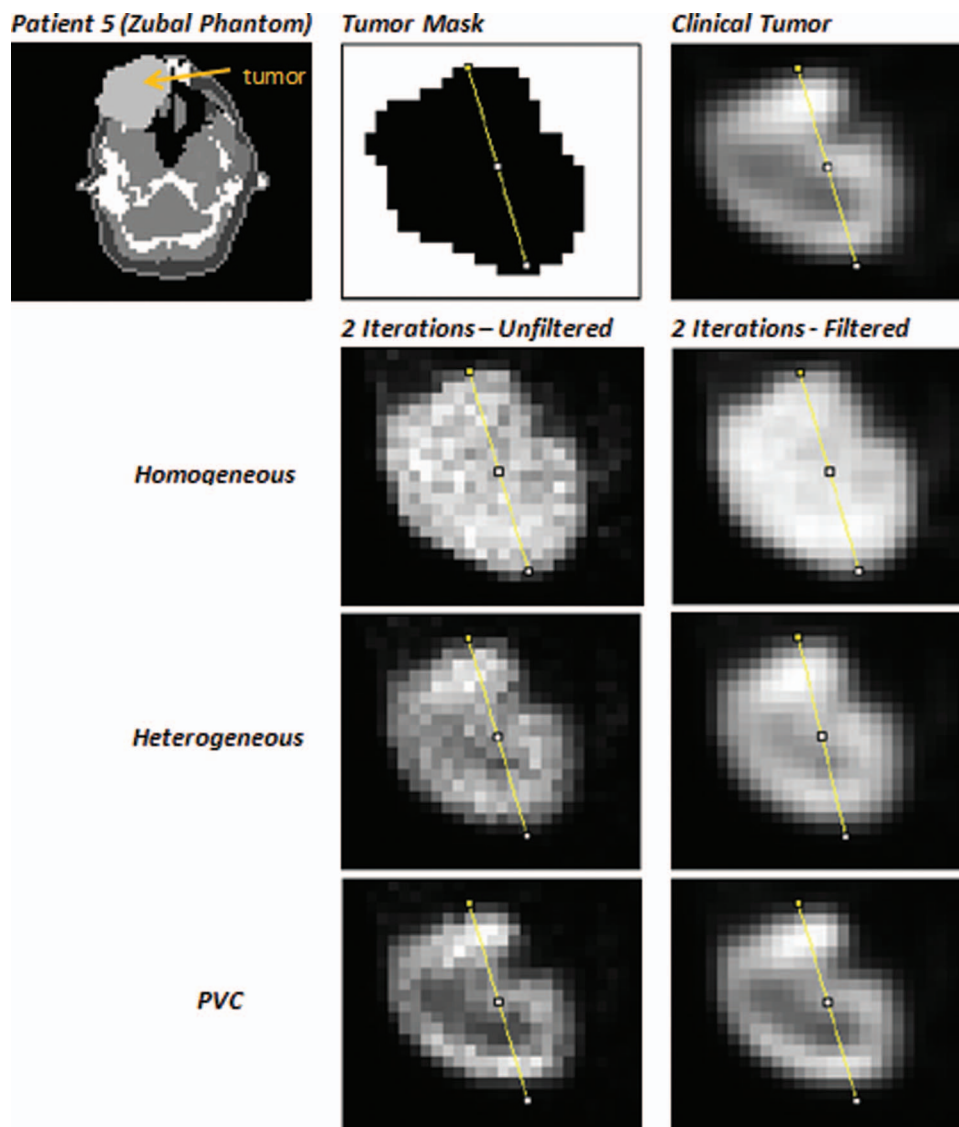


FIG. 4. Patient 5: representation of a central slice of the different tumors simulated cases with and without 3D Gaussian postfiltering. The lines across which the profiles were plotted are represented for comparison reasons with the clinical image.

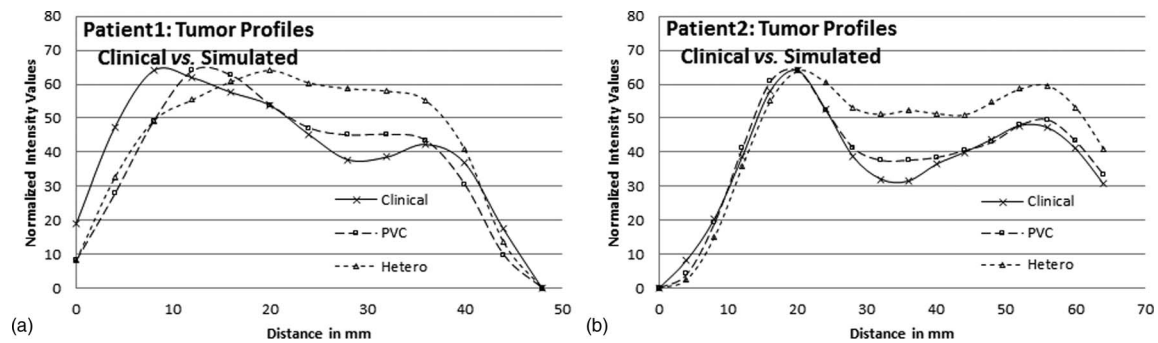


FIG. 5. (a) Comparison of the profiles between the postfiltered simulated data and the clinical tumor for patient 1, and (b) comparison of the profiles between the postfiltered simulated data and the clinical tumor for patient 2.

postfiltering are represented for patient 5. Profiles in the unfiltered images showed large variations, so we included only the profiles of the filtered data with two iterations, which are comparable to the clinical. The simulated homogeneous cases are not included in the profile comparisons as they do not exhibit intratumor heterogeneity. In addition, the clinical PET image is given with its corresponding tumor mask. Figures 5(a) and 5(b) show two examples of such profiles (heterogeneous, PVC, and clinical cases) in two different patients. In Figs. 5(a) and 5(b), the tumor profiles of patient 1 and patient 2 are shown in comparison with the clinical PET image, respectively.

In Fig. 5(a), the intensity of the first peak on the clinical tumor is observed at the distance of 9 mm. In the PVC images, the peak is observed at 13 mm, while in the heterogeneous tumors there is a peak observed at 20 mm. In the region between 30–40 mm, another peak is observed for both the clinical and the PVC cases in contrast to the heterogeneous simulation.

The profiles of the tumor for a second indicative patient (patient 2) are shown in Fig. 5(b). Two different regions are noticed in this case. In the first region, a peak is observed at 15–25 mm and in the second at 55 mm. Additional regions are observed in the PVC data with intensity similar to the clinical image. The second peak shows an intensity 3.5% higher compared to the clinical one, while in the case of the heterogeneous tumor the second peak shows a higher intensity of 20.7%. PVC case seems to best fit the clinical profile.

For the remaining patients the profiles of the filtered simulated data are given in the Appendix [Figs. 6(a)–6(e)]. As it is shown, PVC case of patients 3–7 also seems to best fit the clinical profile.

3.B. Heterogeneity textural features

3.B.1. Local features

In Fig. 7 (in the Appendix), the percentage of the mean differences of the local textural features within the tumors are represented. We have extracted the heterogeneity parameters for all seven patients and the mean differences were calculated in order to extract a general conclusion. The most robust local features are presented namely entropy, homogeneity, and dissimilarity. It can be observed that the PVC simulated tumors provides the lowest differences compared to the clinical im-

ages. More specifically PVC cases show a mean difference of 2.24% for entropy, 9.54% for homogeneity, and 14.29% for dissimilarity.

In Table III the percentage differences of all the patients of the reconstructed (two iterations) filtered data (heterogeneous and PVC) are presented against the clinical data. The highest and the lower differences are marked for every feature taking into account all patients. The highest differences for entropy, homogeneity and dissimilarity are observed in the heterogeneous cases. On the contrary, the lowest values are observed in the PVC cases. In all patients, it is clearly observed that the percentage differences for all local features in the PVC images are quite low. Only for patient 3 the dissimilarity for the PVC case shows a difference higher than 20.0%. However, even this value is lower than the hetero simulations. There are some cases (patient 5 and 6 for homogeneity and dissimilarity) that PVC gave worse results, although those results are lower than 20.0%.

A general trend is observed, where local features in the simulations seem to have smaller variations compared to the features extracted in the clinical PET cases when the input in the activity distribution is corrected for the PVE.

3.B.2. Regional features

In Fig. 8 (see the Appendix), the mean differences of the most stable regional features between simulated and clinical data are presented. In general, we have noticed that regional features and the AUC index have a trend similar to the local features. The PVC simulated tumors exhibit better results than the heterogeneous ones, when compared to the clinical regional features. This means that lower mean differences are found between PVC and clinical images compared to the other simulated cases in intensity variability and in the AUC index. For the size zone variability, the heterogeneous tumors showed better results in the mean differences. More specifically 4.52% difference was observed between heterogeneous and clinical data, while PVC and clinical tumor had a mean difference of 5.21% which is very close to the heterogeneous value. Similar to the local characteristics, in Table IV, the percentage mean differences, of the simulated reconstructed tumors compared to the clinical ones, are presented.

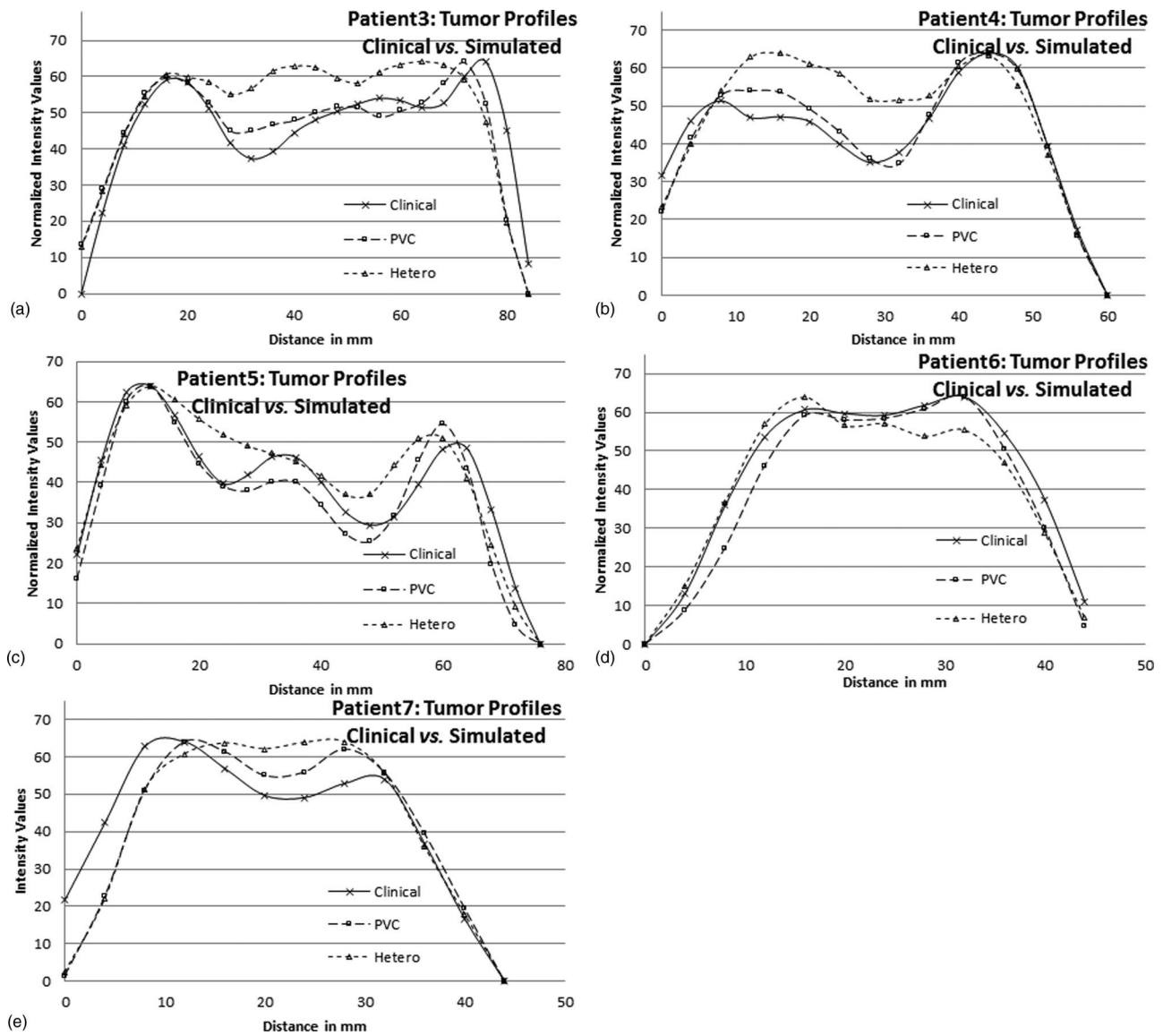


FIG. 6. Comparison of the profiles between the postfiltered simulated data and the clinical tumor (a) for patient 3, (b) for patient 4, (c) for patient 5, (d) for patient 6, and (e) for patient 7.

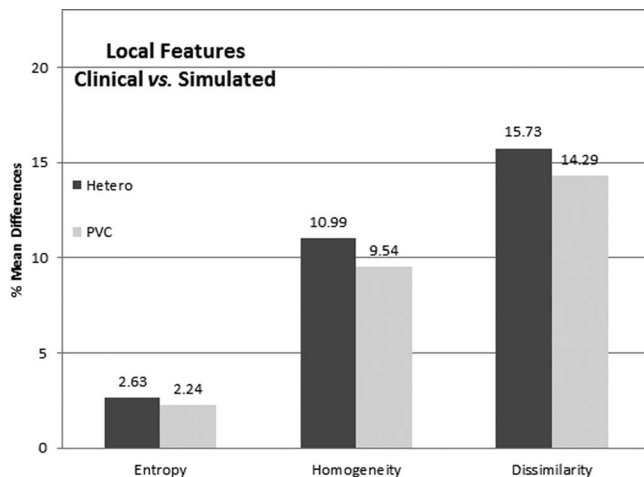


FIG. 7. Histogram of the local features of the mean% differences of all the simulated patients in comparison with the clinical data.

Both the intensity and the size zone variability are quite stable features for all the simulated cases with mean differences smaller than 8.05%. The highest differences are observed for all the features in the heterogeneous tumors, as it was also shown for the local features. Finally, large discrepancies are observed in the AUC index (which has not been tested before for its reproducibility) where PVC data are much better than the other simulated cases, with differences lower than 13% for all seven patients.

3.B.3. Global features

In Table V, the kurtosis, the standard deviation (SD), and the mean intensity values within the tumor of all the patients are presented. The mean difference of each feature is also included. In Fig. 9 (see the Appendix), in accordance

TABLE III. Percentage (%) differences of the local features for the simulated data of all seven patients compared to the clinical PET data. The (%) mean difference of all the cases is also presented.

Patient	Entropy % difference		Homogeneity % difference		Dissimilarity % difference	
	Hetero	PVC	Hetero	PVC	Hetero	PVC
1	0.13	0.35	5.30	3.73	6.14	5.95 ^b
2	10.19 ^a	5.95	24.04 ^a	17.20	24.07	15.96
3	4.68	4.16	17.57	13.37	26.04	23.49
4	0.90	0.88	17.87	12.50	28.85 ^a	18.50
5	1.93	2.41	5.85	9.99	7.54	12.29
6	0.34	1.87	4.24	9.23	9.65	17.17
7	0.27	0.04 ^b	2.03	0.75 ^b	7.80	6.67
Mean	2.63	2.24	10.99	9.54	15.73	14.29

^aThe highest value of the specific feature.

^bThe lowest value of the specific feature.

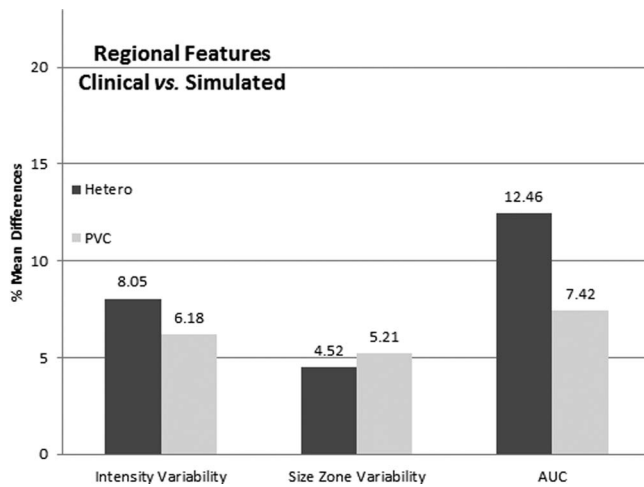


FIG. 8. Histogram of the regional features of the mean% differences of all the simulated patients in comparison with the clinical data.

to the local and the regional features, the percentage mean differences of the global features are presented in histogram.

In general, according to the mean differences, kurtosis and standard deviation gives also better results for the PVC tumors. On the contrary, the mean intensity values are better represented by the heterogeneous simulations with 6.97% difference compared to the clinical tumors. For all the global features, we also observe that the highest differences are observed in the heterogeneous cases, as in local and in regional characteristics. Moreover, it is very interesting that comparing the intensity values of each voxel (voxel-by-voxel comparison) the smallest differences are observed in PVC data.

As shown from the presented differences in Table V, the global features are also better in the PVC simulated cases, closer to the clinical one, except for the mean intensity, which is better reproduced by the heterogeneous tumors. Kurtosis for the PVC data shows differences lower than 20% for all the patients with a mean value lower than 10%.

TABLE IV. Percentage (%) differences of the regional features for the simulated data of all seven patients compared to the clinical PET data. The (%) mean difference of all the cases is also presented.

Patient	Intensity variability % difference		Size zone variability % difference		AUC % difference	
	Hetero	PVC	Hetero	PVC	Hetero	PVC
1	6.79	2.96	1.27	3.37	3.25	5.50
2	8.49	11.22	20.12 ^a	18.81	11.86	4.29
3	2.66	9.42	5.29	2.84	23.74	12.74
4	15.81 ^a	6.33	0.09 ^b	0.55	19.21 ^a	10.42
5	10.32	0.83	3.49	5.81	2.60	14.31
6	11.55	7.34	0.22	0.96	13.24	3.03
7	0.75 ^b	5.19	1.16	4.10	13.33	1.67 ^b
Mean	8.05	6.18	4.52	5.21	12.46	7.42

^aThe highest value of the specific feature.

^bThe lowest value of the specific feature.

TABLE V. Global features for the simulated data of all seven patients compared to the clinical PET data. The mean values of all the cases are also presented.

Patient	Mean intensity % difference		Std difference		Kurtosis % difference		Mean difference voxel-by-voxel comparison	
	Hetero	PVC	Hetero	PVC	Hetero	PVC	Hetero	PVC
1	6.02	14.83	16.79	13.24	7.31	0.45 ^b	23.73	21.4
2	9.37	19.25	35.52 ^a	26.58	8.97	15.42	36.68 ^a	35.18
3	22.52 ^a	1.82	20.02	9.08	50.59 ^b	19.26	23.73	15.56
4	1.19	12.73	15.15	12.11	18.18	7.74	22.73	20.36
5	1.04	17.95	14.34	9.65	17.49	4.56	18.29	19.73
6	7.99	25.02	16.33	5.46 ^b	13.50	15.03	13.45 ^b	20.95
7	0.63 ^b	15.04	15.60	11.85	4.61	6.06	34.83	33.01
Mean	6.97	15.23	19.11	12.57	17.24	9.79	24.78	23.74

^aThe highest value of the specific feature.

^bThe lowest value of the specific feature.

4. DISCUSSION

Freely available datasets are of major importance in medical physics research, since they can provide reference data, methods, and tools to compare results of different teams, as well as overcome resource limitations. However, in the field of nuclear medicine (PET and SPECT), the existence of simulated datasets, including the corresponding clinical images, is very limited in number, realism, and variability. Although MC simulations have played a crucial role in the investigation of several algorithms for image processing and the evaluation of acquisition protocols on clinical systems, no reference dataset exists, which could be exploited by several groups that are working in the field.

In the present study, a database of oncological simulated data was created, based on the GATE toolkit that provides high precision in the physical modeling (using Geant4 code) compared to other MC codes. To overcome computational limitations, we used the GateLab grid for our simulations, resulting in statistics similar to those of clinical protocols. We did not use any speed up methods like VRTs, cuts in physics or accelerated tracking algorithms for the particle

transportation, although their application and effect on results accuracy can be a subject for future research. In addition, only one bed position was simulated and the effect from scattered photons originating from neighboring beds was not assessed.

The developed database, including the sinograms of the simulated data, is freely available to interested researchers for further parameter testing. Thus, several alternative approaches could be tested in reconstruction image correction and image processing at the different simulations of the same patient, for evaluation purposes. Moreover, it can be used to “predict” the clinical output when using an alternative clinical scanner or a different acquisition protocol. Simulated data resulted from simulations using a model of the Philips PET Allegro system. Moreover, datasets of the same patients using the Biograph-6 PET system was included in the database as the simulation scanner has already been accurately simulated by some of the coauthors. The added value and main new result of this work is that, in order to accurately simulate tumor heterogeneity, it is necessary to include a PVC step before introducing PET images as an activity input to GATE simulations. This step constitutes an alternative strategy to what has already been suggested before.¹⁶

The presented database is based on flexible computational anthropomorphic models (NCAT and Zubal). The patient’s variability was taken into account in two different levels. Firstly, the anatomy of the NCAT phantom was adapted to the clinical CT data, and then the ¹⁸F-FDG distribution was extracted based on the corresponding PET images. This procedure is an easily reproducible one if adequate data are available, thus allowing producing a larger dataset. Realistic tumors in shape and in FDG uptake variability were modeled inside the phantoms. The correction of the PVE, which is responsible for the limited resolution in the borders of heterogeneous areas, was tested in the present study, by simulating the realistic tumors with contrast enhancement in the inserted distribution. Previously reported studies had also shown that insertion of the activity map with higher spatial resolution than usual could increase the quality of the simulated data in order to be comparable to the clinical ones.¹⁶ Using original clinical images, without any preprocessing, as an input to a

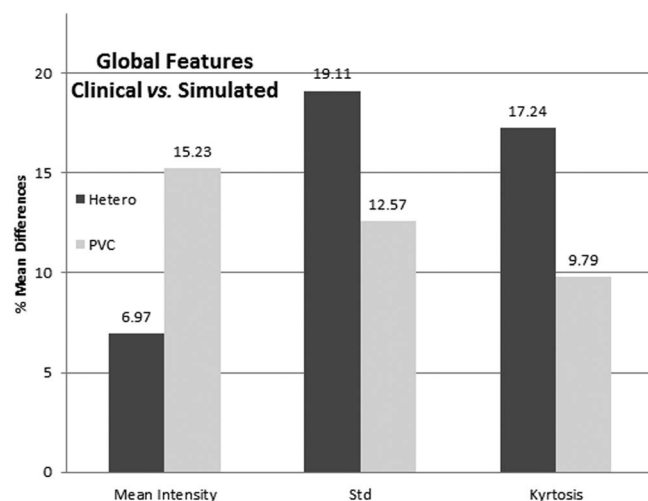


FIG. 9. Histogram of the global features of the mean% differences of all the simulated patients in comparison with the clinical data.

GATE simulation is a common mistake and will lead to more blurred simulated images, since the factors that limit image quality will be practically duplicated in the simulation. PVC activity maps proved to improve the resulting images when compared to clinical data. This led to better results compared to simulations where the heterogeneity activity distribution was directly extracted from PET images. The presented analysis included reconstructed data of two iterations in the reconstruction algorithm. Further investigation comparing the number of the iterations in the reconstruction could be done in whole body simulations. Synthesis and analysis of these two methods in different organs in whole body simulations could increase the overall accuracy of emission tomography simulations.

Our future plans are to support and extend the developed database with SPECT and PET whole body simulated data. In all cases the original corresponding patient, as well as simulated data will be provided. The standardization of the procedure for heterogeneity distribution, which plays a crucial role, will be combined with motion modeling in the phantom, since they are present in clinical data and they definitely affect the obtained clinical images. In this way, it will be possible to provide more qualitative and quantitative acceptable images and assess and/or develop new tools for the evaluation of postprocessing motion correction algorithms, toward improved heterogeneity resolution.

5. CONCLUSION

Our purpose was to standardize a method for accurate/realistic MC simulations within the tumors incorporating patient's characteristics and anthropomorphic computational phantoms. The process and the effect of modeling realistic PET (^{18}F -FDG) tumor simulations, incorporating tumor variability, voxel based heterogeneity and partial volume correction has been analyzed. Seven patients were modeled using the NCAT and the Zubal phantoms, creating seven different datasets of oncology PET situations. Extraction of textural characterization in the activity heterogeneity as well as profiles within the tumors resulted in highly realistic images. PVC simulated data (reconstructed with the STIR software) were comparable to the corresponding clinical images with the less differences.

In conclusion, the oncology database "OncoBase" has been developed from raw data and includes the simulated outputs of clinical data, the respective sinograms (in STIR format) and the corresponding clinical PET data. This database is freely available at <http://www.med.upatras.gr/oncobase/> and will be continuously updated with more datasets from SPECT and PET clinical and preclinical scans.

ACKNOWLEDGMENTS

This study is dedicated to the memory of Nafsika Mousiou, MD who left us so early. This research has been cofinanced by the European Union (European Regional Development Fund—ERDF) and Greek national funds through the Joint Research and Technology Program between Greece and

France (2009–2011); the European Union (European Social Fund) and Greek national resources under the framework of "Archimedes III: Funding of Research Groups in TEI of Athens" project of the "Education and Lifelong Learning" Operational Programme; the European Union (European Social Fund – ESF) and Greek national funds through the Operational Program "Education and Lifelong Learning" of the National Strategic Reference Framework (NSRF) - Research Funding Program: THALES: Investing in knowledge society through the European Social Fund; the European Union (European Regional Development Fund-ERDF) and Greek national funds through the Operational Program "Regional Operational Programme" of the National Strategic Reference Framework (NSRF) – Research Funding Program: Support for research, technology and innovation action in Region of Western Greece; and EU COST action "TD1007 - Bimodal PET-MRI molecular imaging technologies and applications for *in vivo* monitoring of disease and biological processes."

APPENDIX: ADDITIONAL DATA INFORMATION AND FIGURES RESULTED FROM THE PRESENTED ANALYSIS

See Table I and Figures 2, 3, and 6–9.

- a) Author to whom correspondence should be addressed. Electronic addresses: gkagad@gmail.com and George.Kagadis@med.upatras.gr; Telephone: +30 2610 969146; Fax: +30 2610 969166.
- ¹ J. B. Bomanji, D. C. Costa, and P. J. Ell, "Clinical role of positron emission tomography in oncology," *Lancet Oncol.* **2**, 157–164 (2001).
- ² S. Jan *et al.*, "GATE V6: A major enhancement of the GATE simulation platform enabling modelling of CT and radiotherapy," *Phys. Med. Biol.* **56**, 881–901 (2011).
- ³ S. Jan *et al.*, "GATE: A simulation toolkit for PET and SPECT," *Phys. Med. Biol.* **49**, 4543–4561 (2004).
- ⁴ S. Agostinelli *et al.*, "GEANT4: A simulation toolkit," *Nucl. Instrum. Methods Phys. Res. A* **506**, 250–303 (2003).
- ⁵ J. Allison *et al.*, "Geant4 developments and applications," *IEEE Trans. Nucl. Sci.* **53**, 270–278 (2006).
- ⁶ N. Boussion *et al.*, "A multiresolution image based approach for correction of partial volume effects in emission tomography," *Phys. Med. Biol.* **51**, 1857–1876 (2006).
- ⁷ R. L. Harrison, S. D. Vannoy, D. R. Haynor, S. B. Gillispie, M. S. Kaplan, and T. K. Lewellen, "Preliminary experience with the photon history generator module of a public domain simulation system for emission tomography," in *Nuclear Science Symposium and Medical Imaging Conference 1993* (IEEE, 1993), pp. 1154–1158.
- ⁸ C. Lartizien, A. Reilhac, N. Costes, M. Janier, and D. Sappey-Mariner, "Monte Carlo simulation-based design study of a LSO-LuAP small animal PET system," *IEEE Trans. Nucl. Sci.* **50**, 1433–1438 (2003).
- ⁹ F. Perruchot, A. Reilhac, C. Grova, A. C. Evans, and A. Dagher, "Motion correction of multi-frame PET data," in *Nuclear Science Symposium Conference Record* (IEEE, 2004), Vol. 5, pp. 3186–3190.
- ¹⁰ A. Reilhac *et al.*, "PET-SORTEO: Validation and development of database of simulated PET volumes," *IEEE Trans. Nucl. Sci.* **52**, 1321–1328 (2005).
- ¹¹ S. Tomei *et al.*, "OncoPET_DB: A freely distributed database of realistic simulated whole body 18F-FDG PET images for oncology," *IEEE Trans. Nucl. Sci.* **57**, 246–255 (2010).
- ¹² I. Castiglioni, I. Buvat, G. Rizzo, M. C. Gilardi, J. Feuardent, and F. Fazio, "A publicly accessible Monte Carlo database for validation purposes in emission tomography," *Eur. J. Nucl. Med. Mol. Imaging* **32**, 1234–1239 (2005).
- ¹³ C. Tsoumpas *et al.*, "Fast generation of 4D PET-MR data from real dynamic MR acquisitions," *Phys. Med. Biol.* **56**, 6597–6613 (2011).
- ¹⁴ A. Le Maitre *et al.*, "Incorporating patient-specific variability in the simulation of realistic whole-body 18F-FDG distributions for oncology applications," *Proc. IEEE* **97**, 2026–2038 (2009).

- ¹⁵S. Stute *et al.*, "Realistic and efficient modeling of radiotracer heterogeneity in Monte Carlo simulations of PET images with tumors," *IEEE Trans. Nucl. Sci.* **59**, 113–122 (2012).
- ¹⁶S. Stute *et al.*, "Monte Carlo simulations of clinical PET and SPECT scans: Impact of the input data on the simulated images," *Phys. Med. Biol.* **56**, 6441–6457 (2011).
- ¹⁷F. Lamare, A. Turzo, Y. Bizaïs, C. C. Le Rest, and D. Visvikis, "Validation of a Monte Carlo simulation of the Philips Allegro/GEMINI PET systems using GATE," *Phys. Med. Biol.* **51**, 943–962 (2006).
- ¹⁸N. Karakatsanis *et al.*, "Comparative evaluation of two commercial PET scanners, ECAT EXACT HR+ and Biograph 2, using GATE," *Nucl. Instrum. Methods Phys. Res. A* **569**, 368–372 (2006).
- ¹⁹K. Thielemans *et al.*, "STIR: Software for tomographic image reconstruction release 2," *Phys. Med. Biol.* **57**, 867–883 (2012).
- ²⁰D. Visvikis *et al.*, "Characterisation of SUV accuracy in FDG PET using 3-D RAMLA and the Philips Allegro PET scanner," *J. Nucl. Med.* **45**, 103 (2004).
- ²¹P. W. Segars, "Development and application of the new dynamic NURBS-based cardiac-torso (NCAT) phantom," Ph.D. thesis, University of North Carolina, 2001.
- ²²W. Segars and B. Tsui, "4D MOBY and NCAT phantoms for medical imaging simulation of mice and men," in *54th SNM Annual Meeting* (Washington, DC, 2007), Vol. 48, p. 203.
- ²³I. G. Zubal, C. R. Harrell, E. O. Smith, Z. Rattner, G. Gindi, and P. B. Hoffer, "Computerized three-dimensional segmented human anatomy," *Med. Phys.* **21**, 299–302 (1994).
- ²⁴I. G. Zubal, C. R. Harrell, E. O. Smith, and A. L. Smith, "Two dedicated software, voxel-based, anthropomorphic (torso and head) phantoms," in *Proceedings of the International Workshop, National Radiological Protection Board, Chilton, UK, 6–7 July 1995*, edited by P. J. Dimbylow (NRPB, Chilton, 1996), pp. 105–111.
- ²⁵W. P. Segars *et al.*, "Population of anatomically variable 4D XCAT adult phantoms for imaging research and optimization," *Med. Phys.* **40**, 043701 (11pp.) (2013).
- ²⁶P. W. Segars, D. S. Lalush, and B. M. W. Tsui, "Development of an interactive software application to model patient populations in the 4D NURBS-based cardiac torso phantom," in *Nuclear Science Symposium Conference Record* (IEEE, 2000), Vol. 3, pp. 51–55.
- ²⁷M. J. Berger *et al.*, XCOM: Photon Cross Section Database, NIST (available URL: http://www.nist.gov/pml/data/xray_gamma.cfm). Last accessed September 8, 2013.
- ²⁸C. D. Ramos *et al.*, "FDG-PET standardized uptake values in normal anatomical structures using iterative reconstruction segmented attenuation correction and filtered back-projection," *Eur. J. Nucl. Med.* **28**, 155–164 (2001).
- ²⁹M. Hatt, C. Cheze le Rest, A. Turzo, C. Roux, and D. Visvikis, "A fuzzy locally adaptive Bayesian segmentation approach for volume determination in PET," *IEEE Trans. Med. Imaging* **28**, 881–893 (2009).
- ³⁰M. Soret, S. L. Bacharach, and I. Buvat, "Partial-volume effect in PET tumor imaging," *J. Nucl. Med.* **48**, 932–945 (2007).
- ³¹A. S. Kirov, J. Z. Piao, and C. R. Schmidlein, "Partial volume effect correction in PET using regularized iterative deconvolution with variance control based on local topology," *Phys. Med. Biol.* **53**, 2577–2591 (2008).
- ³²O. G. Rousset, Y. Ma, and A. C. Evans, "Correction for partial volume effects in PET: Principle and validation," *J. Nucl. Med.* **39**, 904–911 (1998).
- ³³B. K. Teo *et al.*, "Partial-volume correction in PET: Validation of an iterative postreconstruction method with phantom and patient data," *J. Nucl. Med.* **48**, 802–810 (2007).
- ³⁴J. Tohka and A. Reilhac, "Deconvolution-based partial volume correction in raclopride-PET and Monte Carlo comparison to MR-based method," *Neuroimage* **39**, 1570–1584 (2008).
- ³⁵N. Bousson, C. Cheze Le Rest, M. Hatt, and D. Visvikis, "Incorporation of wavelet-based denoising in iterative deconvolution for partial volume correction in whole-body PET imaging," *Eur. J. Nucl. Med. Mol. Imaging* **36**, 1064–1075 (2009).
- ³⁶A. Reilhac *et al.*, "PET-SORTEO: A Monte Carlo-based simulator with high count rate capabilities," *IEEE Trans. Nucl. Sci.* **51**, 46–52 (2004).
- ³⁷S. Camarasa-Pop, T. Glatard, J. Moscicki, H. Benoit-Cattin, and D. Sarrut, "Dynamic partitioning of GATE Monte-Carlo simulations on EGEE," *J. Grid. Comput.* **8**, 241–259 (2010).
- ³⁸T. Glatard *et al.*, "A virtual imaging platform for multi-modality medical image simulation," *IEEE Trans. Med. Imaging* **32**, 110–118 (2013).
- ³⁹V. Bettinardi *et al.*, "Implementation and evaluation of a 3D one-step late reconstruction algorithm for 3D positron emission tomography brain studies using median root prior," *Eur. J. Nucl. Med. Mol. Imaging* **29**, 7–18 (2002).
- ⁴⁰F. Tixier, M. Hatt, C. C. Le Rest, A. Le Pogam, L. Corcos, and D. Visvikis, "Reproducibility of tumor uptake heterogeneity characterization through textural feature analysis in 18F-FDG PET," *J. Nucl. Med.* **53**, 693–700 (2012).
- ⁴¹P. E. Galavis, C. Hollensen, N. Jallow, B. Paliwal and R. Jeraj, "Variability of textural features in FDG PET images due to different acquisition modes and reconstruction parameters," *Acta Oncol.* **49**, 1012–1016 (2010).
- ⁴²F. Tixier *et al.*, "Intratumor heterogeneity characterized by textural features on baseline 18F-FDG PET images predicts response to concomitant radiochemotherapy in esophageal cancer," *J. Nucl. Med.* **52**, 369–378 (2011).
- ⁴³F. H. van Velden *et al.*, "Evaluation of a cumulative SUV-volume histogram method for parameterizing heterogeneous intratumoural FDG uptake in non-small cell lung cancer PET studies," *Eur. J. Nucl. Med. Mol. Imaging* **38**, 1636–1647 (2011).